

Methods to assess bioresorbable vascular scaffold devices behaviour after implantation

Alberto Pernigotti, Elisabetta Moscarella, Giosafat Spitaleri, Claudia Scardino, Kohki Ishida, Salvatore Brugaletta

Hospital Clinic, Institut Clinic Cardiovascular, IDIBAPS, Barcelona, Spain

Contributions: (I) Conception and design: All authors; (II) Administrative support: All authors; (III) Provision of study materials or patients: All authors; (IV) Collection and assembly of data: All authors; (V) Data analysis and interpretation: All authors; (VI) Manuscript writing: All authors; (VII) Final approval of manuscript: All authors.

Correspondence to: Salvatore Brugaletta, MD, PhD. Hospital Clinic, Institut Clinic Cardiovascular, IDIBAPS, Carrer Villarroel 170, Barcelona, Spain. Email: sabrugal@clinic.cat.

Abstract: Bioresorbable vascular scaffolds (BRS) represent a novel approach for coronary revascularization offering several advantages as compared to current generation DES, potentially reducing rate of late adverse events and avoiding permanent vessel caging. Nevertheless, safety concerns have been raised for an increased risk of scaffold thrombosis (ScT) in both early and late phases, probably related to a suboptimal scaffold implantation. In this context, the use of different imaging methodologies has been strongly suggested in order to guarantee an optimal implantation. We herein analyze the different imaging methodologies available to assess BRS after implantation and at follow-up.

Keywords: Scaffold; intravascular ultrasound (IVUS); echogenicity; virtual histology-IVUS (VH-IVUS); optical coherence tomography (OCT); multislice coronary tomography (MSCT)

Submitted Apr 24, 2017. Accepted for publication Jun 05, 2017.

doi: 10.21037/jtd.2017.06.110

View this article at: <http://dx.doi.org/10.21037/jtd.2017.06.110>

Introduction

Bioresorbable vascular scaffolds (BRS) represent the so-called fourth revolution in the field of interventional cardiology, after the introduction of bare metal stents, first- and second-generation drug-eluting stents (DES). In recent years, a big advance has been made in developing BRS and there are currently numerous devices available for preclinical or clinical use.

These devices have several potential advantages over current generation DES. First, this novel technology provides transient vessel support with drug delivery capability without the long-term limitations of metallic stents, such as permanent vessel caging, that may lead to late acquired malapposition, thus potentially reducing the rate of late adverse events. Second, once the absorption process is complete, BRS allow the recovery of a normal vascular

function, with physiological vasomotion and a theoretical increase of the vessel area (late lumen enlargement) (1). Moreover, BRS implantation allows surgical anastomosis in the treated coronary segment, whereas traditional metallic stents preclude it (2). Finally, regarding clinical follow-up, BRS may be non-invasively evaluated by multislice coronary tomography (MSCT) that can visualize the vascular lumen in the treated area without the blooming effect observed with metallic stents (3).

Despite this initial enthusiasm, safety concerns have been raised about increased risk of scaffold thrombosis (ScT) in both early and late phases probably related to suboptimal scaffold implantation (4). A specific interventional strategy with adequate lesion preparation and the systematic scaffold post-dilatation may be required to guarantee an optimal scaffold implantation (5). In this context, use of different imaging techniques has been strongly suggested

for BRS implantation in order to confirm optimal scaffold expansion, to exclude edge dissections, struts malapposition or underexpansion. Furthermore, imaging technique may evaluate at follow-up scaffold reabsorption and vessel changes over time.

We herein analyze the different imaging methodologies available to assess BRS after implantation and at follow-up.

Quantitative coronary angiography (QCA)

Coronary angiography is the most important method for assessing BRS implantation. As well as for conventional stent, at least two different projections with at least 30° difference for the right coronary artery and 3 different projections with at least 30° difference for the left coronary artery must be acquired before and after BRS implantation. The treated segment and the 5 mm proximal and distal to scaffold edges should be analyzed. As the bioresorbable devices are radiolucent, the QCA analysis may be performed visualizing the metallic markers of the scaffold.

The following parameters can be measured.

Acute recoil

It is defined as the difference between the mean diameter of the BRS delivery balloon (or, in case of post-dilatation, mean diameter of post-dilatation balloon) at the highest pressure and the mean lumen diameter (MLD) of the stented segment after balloon deflation. It can be expressed as absolute or relative value. The acute recoil is an important parameter in relation to the success of a PCI in acute and long-time period, as it has a direct impact on minimum stent area (MSA). A MSA less than 5.0 mm² is associated with high probability of in-stent restenosis (6).

The acute recoil of Absorb BVS 1.1 (Abbott Laboratories, Abbott park, Illinois, USA) in the Absorb Cohort B trials and DESolve Nx BRS (Elixir Medical, Sunnyvale, California, USA) were 6.7%±6.4% and 6.4%±4.6%, respectively (7,8). These values are not dissimilar to those of metallic stent, showed in a Japanese study of 154 lesions comparing the biolimus eluting stent (Nobori stent, Terumo, Tokyo, Japan), cobalt chromium everolimus eluting stent (Xience V stent, Abbott Vascular, Santa Clara, CA, USA) and platinum chromium everolimus-eluting stent (EES) (Promus Element stent, Boston Scientific, Natick, MA, USA). Acute recoil was 6.7%±5.5%, 10.1%±6.9% and 6.5%±4.8%, respectively (9,10).

Curvature and angulation

“Curvature” is defined as the infinitesimal rate of change in the tangent vector at each point of the center-line. This measurement has a reciprocal relationship to the radius of a perfect circle defined by the curve at each point. The curvature value is calculated as 1/radius of the circle in cm⁻¹. “Angulation” is defined as the angle in degrees that the tip of an intracoronary guidewire would need to reach the distal part of a coronary bend (11).

Implantation of a stent/scaffold in a coronary artery may result in change of vessel geometry which can lead to increase shear stress and, finally, exacerbated neo-intimal response and asymmetrical patterns of in-stent restenosis (12,13). However, studies conducted with second generation DES failed to demonstrate a relationship between clinical outcome and vessel curvature and angulation (14).

Data on BRS showed that these devices generate an acute geometrical change after its implantation; however, at follow-up, once reabsorption is completed, there is a partial restoration of coronary geometry, as curvature and angulation values are more similar to pre-implantation values. The clinical implication of these findings has to be further investigated (15,16).

Vasomotion

Vasomotion is the response of coronary artery to vasoactive agents, such as nitrate and acetylcholine (Ach), which can produce vasodilatation or vasoconstriction. While nitrates have a direct relaxing effect on smooth muscle cells of the vascular wall (17), Ach dilate normal arteries by promoting release of a vasorelaxing substance from the endothelium (endothelium-derived relaxing factor); conversely, if the endothelium is removed or damaged experimentally, Ach provoke vasoconstriction (18). In order to assess vasomotion, an intracoronary bolus injection of nitroglycerine (200 µg) is usually administered through the guiding catheter with two angiograms, one before and another after nitrate administration. Ach is infused via a microcatheter, placed 8–12 mm proximal to the stent/scaffold. Incremental doses of Ach (0.36, 3.6 and 18 µg/mL) are applied into the coronary artery at a rate of 2 mL/min for 5 min per dose. The highest possible dose should be assessed. MLD should be determined before and after infusion of nitrates or Ach in the scaffolded area and in proximal/distal (5-mm segment) edges. MLD should be averaged from at least 2

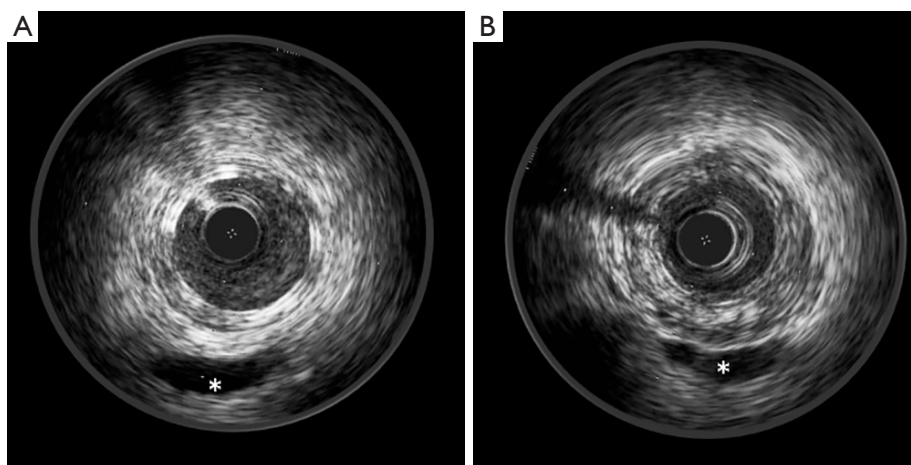


Figure 1 IVUS images of an Absorb BVS after implantation (A) and at 3-year follow-up (B). Note how Absorb BVS struts appear as a double layer structure after implantation and how they disappear at 3-year follow-up. *, indicates a vein. IVUS, intravascular ultrasound.

projections, and the relative change from baseline should be noted. Vasomotor response to Ach or nitroglycerine is defined as a change of at least 3% or more of the MLD after injection (19). This percentage represents the error rate inherent to angiography in evaluating lumen diameter.

In Absorb Cohort B, patients treated with BRS exhibited at 24 months a significant increase, on average, in the MLD after Ach administration compared with patients at 12 months [+6.16%, 95% CI, (-1.07, +13.14) *vs.* -6.41%, 95% CI, (-11.74, -1.17); $P=0.006$] (20). On the contrary, the Absorb II trial, which compared Absorb BVS with EES, did not show a statistically difference in vasomotion at 3 years follow up (Absorb BVS group 0.047 ± 0.109 mm *vs.* EES group 0.056 ± 0.117 mm) (21). With regards to Magmaris scaffold (Biotronick, Bülach, Switzerland), the median percentage change in MLD between pre- and post-Ach was -2.6% (IQR: -6.4% to -0.6%, mean: $-5.1\pm 7.7\%$) at 6 months and -3.4% (IQR: -9.4% to 3.2%, mean: $-3.4\pm 11.0\%$) at 12 months (22).

Late lumen loss (LLL)

LLL is defined as the difference between minimum lumen diameter at post-procedure and at follow-up. For lumen diameter reduction, this will be a positive number; in case of increase in lumen size, this will be a negative number. This parameter is of importance in assessing the behavior of the scaffold, as it represents the reduction of the lumen of the scaffold due to neointimal proliferation, which is the main

mechanism of in-scaffold restenosis (23).

Absorb II trial showed a larger LLL in the Absorb BVS group than in the Xience group (0.37 ± 0.45 *vs.* 0.25 ± 0.25 mm, at 3-year follow-up). In Biosolve II trial, Magmaris device showed a LLL of 0.20 ± 0.21 mm at 6 months and a 0.25 ± 0.22 mm at 12 months.

Although BRS could theoretically generate negative value of LLL (which translates into a late lumen gain and an increase in minimal lumen diameter) once resorption is completed, these trials did not show it. Longer follow-up would be needed to investigate it further.

Gray-scale intravascular ultrasound (IVUS)

IVUS images are obtained by ultrasounds waves generated by contraction and expansions of a piezoelectric crystal mounted on the tip of a catheter. After reflection from coronary tissue, part of the ultrasound energy returns to the transducer, producing an electrical impulse which is converted into an image.

For a 20 to 40 MHz IVUS transducer, the typical resolution is 80 microns axially and 200 to 250 microns laterally. As compared to angiography, it provides additional information about coronary anatomy and scaffold implantation. Correct evaluation of IVUS parameters may greatly improve PCI result, especially in complex anatomy (24).

At IVUS, Absorb struts appear as a double layer structure, which disappear during resorption (*Figure 1*).

The IVUS main parameters are the following.

Eccentricity and symmetry indices

Eccentricity index is defined as the ratio between minimum and maximum diameter of the lumen, scaffold or vessel. Symmetry index is defined as the ratio between the difference of maximum and minimum scaffold diameter divided by maximum scaffold diameter [(Dmax – Dmin)/Dmax].

The MUSIC trial showed that an eccentricity index ≥ 0.7 may positively contribute to the immediate and 6-month clinical and angiographic outcomes after PCI (25,26). Moreover, other studies have shown that asymmetrical expansion may be a determinant of thrombus formation after stent implantation (27).

In Absorb II trial, the Absorb BVS group exhibited a higher asymmetry and a lower eccentricity index than the EES group: scaffold/stent asymmetry index was 0.33 in Absorb BVS and 0.27 in EES, and device eccentricity index after implantation was <0.7 in 27.3% in Absorb group and 4.5% in EES group. Post-procedural devices asymmetry and eccentricity were hypothetically related to higher event rates as device-oriented composite endpoint was higher in asymmetrical device, but without statistical significance due to low events rate (28).

A non-randomized multicentre study comparing Absorb BVS and DESolve devices in 72 patients showed a higher mean eccentricity index for Absorb BVS scaffold (0.85 ± 0.05 vs. 0.80 ± 0.05 , $P < 0.01$). DESolve is more prone to asymmetric expansion probably because of its intrinsic structural characteristics (29).

Lumen, vessel and scaffold area

Lumen and vessel areas are depicted on lumen and on external elastic membrane on the IVUS cross section, respectively. Their ratio represents lumen area stenosis. After BRS implantation, scaffold and lumen area should be the same. These parameters can be drawn per frame and mean and minimum values can be expressed per segment or per scaffold. Scaffold minimal area is related to a good result of a PCI, as MLA less than 5.0 mm^2 is associated with a high rate of target lesion restenosis in metallic platform stent trials (6).

Neointima hyperplasia

It is defined as the difference between scaffold area and

lumen area at follow-up.

Incomplete scaffold apposition (ISA)

It is defined as a separation of one or more scaffold strut from the vessel wall. It can be observed acutely, after the implantation, or at follow-up. In this latter case, it is called late acquired incomplete apposition if not present after implantation. This parameter is better recognized with OCT evaluation. Studies demonstrated that ISA after DES implantation may have an impact on events rate in long-term follow-up, in particular on very late stent thrombosis (30).

Edge effects

Edge effect is defined as a tissue proliferation at proximal and distal edge of the scaffold. Five-mm proximal and distal device edges are taken in consideration. Typically, is observed at proximal edge as a focal restenosis (31).

Echogenicity

The echogenicity data, derived from the IVUS greyscale, have been used to evaluate plaque composition (32) and, more recently, BRS reabsorption after their implantation (33).

The mean grey-value of the adventitia represents the reference to classify the values of echogenicity (hypoechoic or hyperechoic) inside external elastic membrane. Adventitia is defined as a layer extending from 0.2 to 0.5 mm outside of the external elastic membrane. A dedicated QCU software (CURAD) is used in detecting lumen-intima and external elastic membrane border (34). After the tissue identification process, the echogenicity value is calculated for the entire investigated segment.

Echogenicity has been used to follow the bioresorption process of the Absorb BVS device, as PLLA device has high echogenicity and its structure can be well visualized by ultrasound. As a surrogate for bioresorption, the percentage differential echogenicity significantly decreased from $13.8\% \pm 4.7\%$ after BRS implantation, to $11.6\% \pm 5.6\%$ at 3 years ($P < 0.0001$) (16) (Figure 2).

DREAMS device (Biotronik, Bülach, Switzerland), a previous version of Magmaris, was investigated before and after implantation and at 6-, 12- and 18-month follow up in an analogue method in the BIOSOLVE-I trial. The

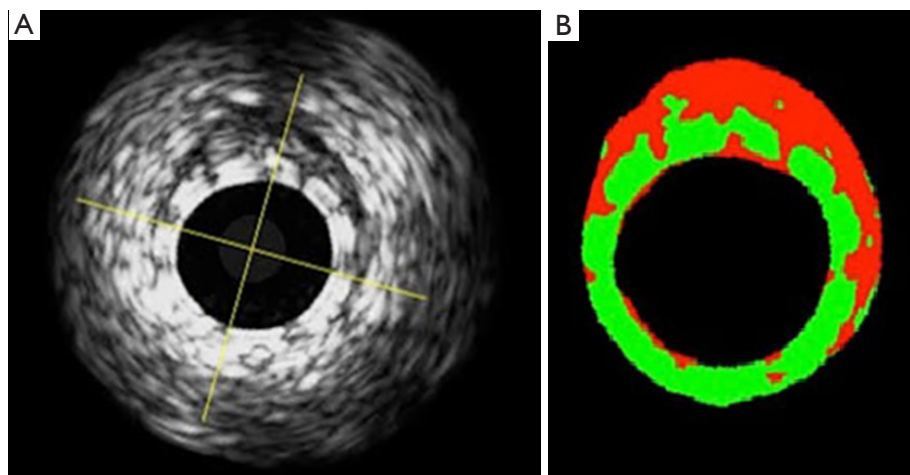


Figure 2 (A) Shows a grayscale IVUS image of an Absorb BVS immediately after implantation. The echogenicity software recognizes the Absorb BVS struts as hyper-echogenic tissues, depicting them as green in (B), whereas hypo-echogenic tissue is red. IVUS, intravascular ultrasound.

analysis demonstrated a progressive absorption over time, especially in the first 6 months after implantation (16).

Virtual histology (VH)

VH-IVUS is an invasive imaging modality that uses radiofrequency ultrasound backscatter data to identify plaque components (e.g., necrotic core, dense calcium, fibrous, and fibrofatty tissues) (35).

A 20-MHz, 3.2-F catheter (Eagle Eye, Volcano Corporation, Rancho Cordova, California, USA) or a 45-MHz (Revolution, Volcano Corporation) is advanced in the target coronary artery, distal to the region of interest (at least 5-mm distal the scaffolded area), after the administration of intracoronary nitroglycerin. During pullback, grayscale IVUS images are recorded and raw radiofrequency data are captured at the top of the R wave; reconstruction of the color-coded map by an IVUS-VH data recorder is then performed (InVision Gold, Volcano Corporation) (36).

IVUS-VH plaque components are colour coded as dense calcium (white), necrotic core (red), fibrofatty (light green), or fibrous tissue (dark green) and reported as absolute and relative values.

Scaffolds struts are detected as areas of dense calcium and necrotic core, due to the strong backscattering properties of the polymer. For this reason, VH-IVUS has been used in the evaluation of the polymer reabsorption process analysing the variation of the backscattering signal between

post-procedure and follow-up (Figure 3).

The analysis of the ABSORB Cohort B study showed that the mean dense calcium areas decreased progressively from 29.84 mm² (post implantation), to 21.52 mm² (3-year follow-up). The average necrotic core areas have a similar behaviour, reducing from 31.31 mm² after implantation to 26.49 mm² at 3-year follow-up. A sharp decrease in dense calcium and necrotic core areas between 24 and 36 months can be also detected, which may reflect the end of the inflammatory process, with regression of the plaque behind the struts (37). Local elution of everolimus has been demonstrated to have autophagic capabilities on macrophages, with a subsequent effect of diminishing necrotic core formation, inflammation, and thrombosis, which can contribute to necrotic core reduction (38).

Optical coherence tomography (OCT)

OCT, using infrared light source, has a resolution of 10 μm which is about ten times higher than IVUS, allowing a more detailed visualisation of intracoronary structures.

This intravascular imaging evaluation includes different parameters allowing a quantitative and qualitative analysis of the scaffolded vessel.

While post implantation measurements are easily identified since strut area is imaged as a central black core and a light-scattering frame border, detection of the main quantitative measurements at follow-up examination, such as strut area, lumen area, scaffold area, ISA area

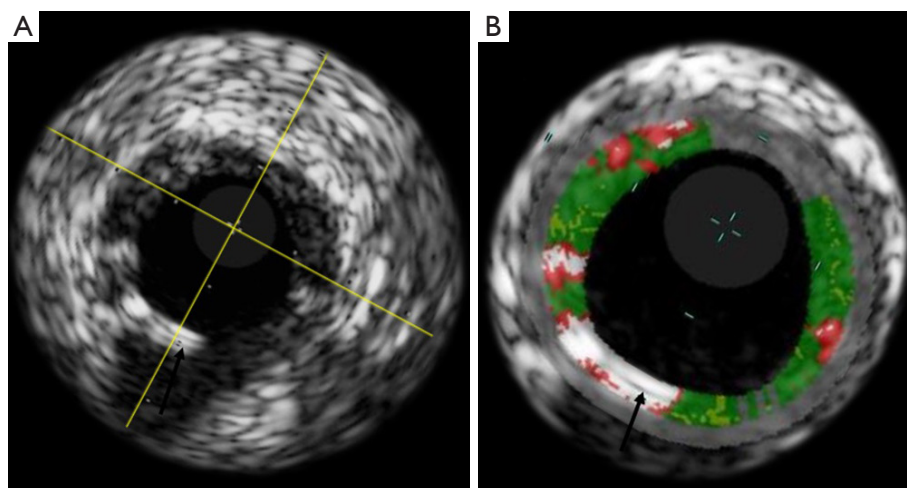


Figure 3 (A) Shows a greyscale IVUS image of an Absorb BVS after implantation. In (B), the VH is superimposed to the greyscale image, showing how the Absorb BVS struts (black arrows) are recognized by the software as dense calcium (white) and necrotic core (red). IVUS, intravascular ultrasound, VH, virtual histology.

and neointimal area, require different rules as metallic stent (39). As another article in this journal's issue is talking about qualitative and quantitative OCT parameters, we will now focus on the reabsorption OCT parameters of BRS.

While metal struts are preserved and there is a clear definition between stent and lumen contour with a shadow behind the metal, Absorb BVS struts, made of poly-lactic acid, do not create a shadow behind each strut and at long-term follow-up, are no longer visible, as the struts are filled by fibrous tissue with similar optical properties as the underlying fibrous layer. Consequently, it is impossible to distinguish between strut area, neointimal area, and underlying plaque. The vascular structure observed at the scaffolded segment, a product of the solidification of underlying plaque, biodegraded struts, and neointima, is similar to a native atherosclerotic plaque and it was defined as neoplague. In order to evaluate and separate the different composition of the scaffolded vessel and the underlying neoplague elements, an indirect assessment has been provided. It is based on the signal-rich layer, which consisted of the neointimal layer, resorbed struts, and pre-existing fibrous tissue (40).

Both in-man and animal model studies described Absorb BVS 1.0 struts features during the different stages of the absorption process (41,42). Immediately after implantation, the polymeric struts are clearly identified. The bright reflection borders contrast with a black core, giving the typical aspect called "preserved box". This is

the OCT appearance of intact PLLA-PDLLA structure. After 6 months, there is a gradual disappearance of this pattern, which is considered to be the initial stages of the bioresorption process. This aspect has been called "open box pattern", where there is an opening of the extremities of the box in its short axis. The "dissolved bright box" appearance, with partially visible bright spot and poorly defined contours, is considered the further stages of bioresorption. "Dissolved black box", a black spot with poorly defined contours and no box-shaped, is the fourth and later stage which correspond Absorb BVS degradation and vessel wall integration.

For the Absorb BVS 1.1, which is currently on the market, it is however impossible to get a clear differentiation between these phases, due to a probable different bioresorption process. Nevertheless, the progression to the complete absorption is very similar, as demonstrated by Onuma *et al.* (39). In this study has been done a correlation between the Absorb BVS 1.1 absorption process at OCT, with that observed in histological analysis with porcine models: at 24 months, the strut void is covered and encapsulated by neointimal tissue in both models (polylactide is no longer detectable in histologic section). At 36 months, the proteoglycan is replaced by connective tissue so that the strut footprint is indiscernible at 4 years in OCT and histology analysis.

In magnesium BRS, these typical patterns are not observed, as magnesium has completely different structural

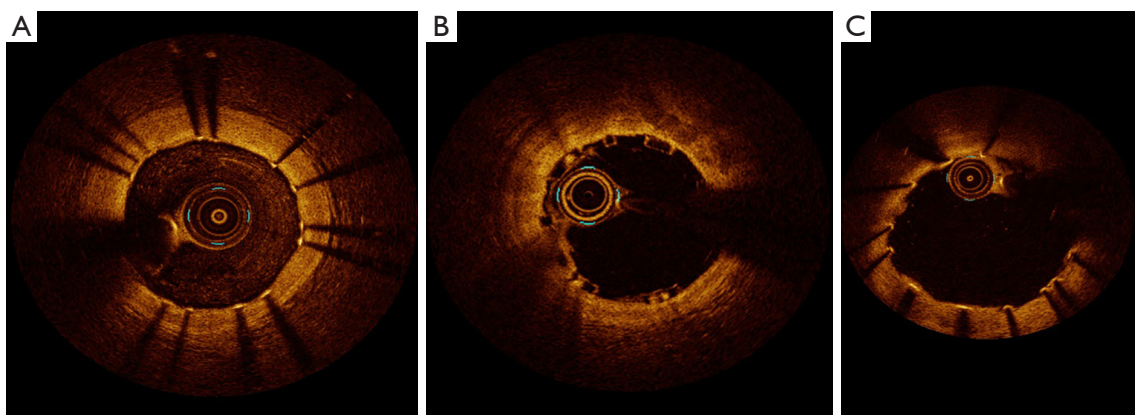


Figure 4 OCT aspect of metallic platform stent (A), Absorb BVS (B) and Magmaris (C), after implantation. The PLLA/PDLLA struts of Absorb BVS device do not determine a shadow behind in the OCT image (B), as the light can cross them. On the contrary, Magmaris scaffold (C), as well as metallic platform stent (A), creates a shadow behind the metallic struts. OCT, optical coherence tomography.

properties than PLLA-PDLLA. In Biosolve II trial, after implantation, Magmaris has similar appearance to conventional metallic platform stent, generating a shadow, which reduces the visualization of the underlying vessel structures. This phenomenon tends to be gradually reduced following absorption process until completely disappearing (21) (*Figure 4*).

MSCT

As not made of metal, PLLA-PDLLA devices allow non-invasive evaluation of the treated coronary segment by MSCT without the blooming effect observed with metallic stents (43). BRS can be recognized by the metallic markers at both ends of the devices, made of platinum, gold or tantalum. QCA-like parameters can be obtained, as well as monitoring of scaffold absorption. In the Absorb Cohort A 25 patients underwent MSCT as an optional investigation at 18 months and 18 patients at 60 months. Quantitative analysis of the scaffolded segment was feasible in all patients and the assessment of the lumen by MSCT revealed the persistence of the lumen area up to 5 years after the Absorb BVS implantation with a non-significant decrease in plaque area (44).

There have been concerns about the potential risk of dislodgement of metallic markers spheres with potential embolization into the coronary bed after complete bioresorption of the device. This phenomenon could be a problem for the risk of coronary complication, but also for the impossibility to discern the segment of implant of the BRS completely absorbed. A retrospective study analyzed

MSCT performed at 18 months after the procedure of 168 coronary lesion treated with Absorb BVS 1.0 and 1.1, in order to establish the persistent presence of scaffold metallic markers. No embolization was found and all the radio-opaque markers were correctly detected at implant site (45). MSCT demonstrated a good reproducibility in performing metallic markers detection.

MSCT has been also adopted in studying the behaviour of side branches covered by an Absorb BVS (46). This methodology allows analysing the rate of side branch occlusion, immediately after Absorb BVS implantation, its clinical impact, the predictors of side branch occlusion and the fate of such side branches at 6-month follow-up using MSCT.

Magnetic resonance angiography (MRA)

MRA can be used for the visualization of both cardiac vessel and lumen, but it is not yet recognized and/or recommended as follow-up diagnostic procedure in patients treated with metallic platform stent as these devices are known to shield off the radio frequency field during magnetic resonance imaging (MRI) signal excitation and data acquisition. Conversely, BRS allow in-scaffold assessments of the coronary lumen because, after their bioresorption, only the radio-opaque markers at each edge of the stent remained visible, not interfering MRI (47).

The current medical literature does not reveal large scale trials about BRS detection with MRA, but only *in vitro* study (48) and a small number of in-vivo case reports (49,50), mainly studying Absorb BVS and DESolve devices. In

particular, Reiss and colleagues conducted an investigation consistent in an in-vitro assay demonstrating the feasibility of MRA to analyse the Absorb device and a second *in vivo* examination, conducted on two patients in which the BRS was correctly identified without significant artefacts.

However, as described in all *in vivo* examination (49,50), MRI can visualize with high definition only the proximal and mid sections of the coronary artery vessels. The poor assessment of distal coronary segments and of the platinum markers of BRS represents the most important limitation of this technology in this field. This aspect should be resolved in future with a further improvement of MRI sequences.

Conclusions

Coronary imaging is important in the assessment of BRS, either for optimizing their implantation or for follow-up evaluation. Knowledge of different aspects of these methodologies is essential in avoiding scaffold malapposition and underexpansion and in preventing short and long-term adverse events.

Acknowledgements

None.

Footnote

Conflicts of Interest: The authors have no conflicts of interest to declare.

References

- Oberhauser JP, Hossainy S, Rapoza RJ. Design principles and performance of bioresorbable polymeric vascular scaffolds. *EuroIntervention* 2009;5 Suppl F:F15-22.
- Tarantini G, Saia F, Capranzano P, et al. SICI-GISE Position paper: Use of Absorb BVS in clinical practice. *G Ital Cardiol (Rome)* 2016;17:28S-44.
- Onuma Y, Dudek D, Thuesen L, et al. Five-year clinical and functional multislice computed tomography angiographic results after coronary implantation of the fully resorbable polymeric everolimus-eluting scaffold in patients with de novo coronary artery disease: the ABSORB cohort A trial. *JACC Cardiovasc Interv* 2013;6:999-1009.
- Brugaletta S, Pernigotti A. Absorb BVS: quo vadis? *G Ital Cardiol (Rome)* 2016;17:45S-6.
- Ortega-Paz L, Capodanno D, Gori T, et al. Predilation, sizing and post-dilation scoring in patients undergoing everolimus-eluting bioresorbable scaffold implantation for prediction of cardiac adverse events: development and internal validation of the PSP score. *EuroIntervention* 2017. [Epub ahead of print].
- Sonoda S, Morino Y, Ako J, et al. Impact of final stent dimensions on long-term results following sirolimus-eluting stent implantation: serial intravascular ultrasound analysis from the SIRIUS trial. *JACC* 2004;43:1959-63.
- Onuma Y, Serruys PW, Gomez J, et al. Comparison of in vivo acute stent recoil between the bioresorbable everolimus-eluting coronary scaffolds (revision 1.0 and 1.1) and the metallic everolimus-eluting stent. *Catheter Cardiovasc Interv* 2011;78:3-12.
- Verheye S, Ormiston JA, Stewart J, et al. A next-generation bioresorbable coronary scaffold system: from bench to first clinical evaluation: 6- and 12-month clinical and multimodality imaging results. *JACC Cardiovasc Interv* 2014;7:89-99.
- Ota T, Ishii H, Sumi T, et al. Impact of coronary stent designs on acute stent recoil. *J Cardiol* 2014;64:347-52.
- Kitahara H, Waseda K, Yamada R, et al. Acute stent recoil and optimal balloon inflation strategy: an experimental study using real-time optical coherence tomography. *EuroIntervention* 2016;12:e190-8.
- Gomez-Lara J, Garcia-Garcia HM, Onuma Y, et al. A comparison of the conformability of everolimus-eluting bioresorbable vascular scaffolds to metal platform coronary stents. *JACC Cardiovasc Interv* 2010;3:1190-8.
- Gyöngyösi M, Yang P, Khorsand A, et al. Longitudinal straightening effect of stents is an additional predictor for major adverse cardiac events. Austrian Wiktor Stent Study Group and European Paragon. *J Am Coll Cardiol* 2000;35:1580-9.
- Wentzel JJ, Krams R, Schuurbiens JC, et al. Relationship between neointimal thickness and shear stress after wall stent implantation in human coronary arteries. *Circulation* 2001;103:1740-5.
- Gomez-Lara J, Heo JH, Brugaletta S, et al. Risk of target lesion failure in relationship to vessel angiographic geometry and stent conformability using the second generation of drug-eluting stents. *Am Heart J* 2011;162:1069-1079.e2.
- Gomez-Lara J, Brugaletta S, Farooq V, et al. Angiographic geometric changes of the lumen arterial wall after bioresorbable vascular scaffolds and metallic platform stents at 1-year follow-up. *JACC Cardiovasc Interv*

- 2011;4:789-99.
16. Waksman R, Prati F, Bruining N, et al. Serial observation of drug-eluting absorbable metal scaffold: multi-imaging modality assessment. *Circ Cardiovasc Interv* 2013;6:644-53.
 17. Torfgård KE, Ahlner J. Mechanisms of action of nitrates. *Cardiovasc Drugs Ther* 1994;8:701-17.
 18. Ludmer PL, Selwyn AP, Shook TL, et al. Paradoxical vasoconstriction induced by acetylcholine in atherosclerotic coronary arteries. *N Engl J Med* 1986;315:1046-51.
 19. Hofma SH, van der Giessen WJ, van Dalen BM, et al. Indication of long-term endothelial dysfunction after sirolimus-eluting stent implantation. *Eur Heart J* 2006;27:166-70.
 20. Brugaletta S, Heo JH, Garcia-Garcia HM, et al. Endothelial-dependent vasomotion in a coronary segment treated by ABSORB everolimus-eluting bioresorbable vascular scaffold system is related to plaque composition at the time of bioresorption of the polymer: indirect finding of vascular reparative therapy? *Eur Heart J* 2012;33:1325-33.
 21. Serruys PW, Chevalier B, Sotomi Y, et al. Comparison of an everolimus-eluting bioresorbable scaffold with an everolimus-eluting metallic stent for the treatment of coronary artery stenosis (ABSORB II): a 3 year, randomised, controlled, single-blind, multicentre clinical trial. *Lancet* 2016;388:2479-91.
 22. Haude M, Ince H, Abizaid A, et al. Sustained safety and performance of the second-generation drug-eluting absorbable metal scaffold in patients with de novo coronary lesions: 12-month clinical results and angiographic findings of the BIOSOLVE-II first-in-man trial. *Eur Heart J* 2016;37:2701-9.
 23. Harrison RW, Radhakrishnan V, Lam PS, et al. Rationale and design of the East-West late lumen loss study: Comparison of late lumen loss between Eastern and Western drug-eluting stent study cohorts. *Am Heart J* 2016;182:103-10.
 24. Sarno G, Onuma Y, Garcia Garcia HM, et al. Catheter IVUS radiofrequency analysis in the evaluation of the polymeric struts of the bioabsorbable everolimus-eluting device during the bioabsorption process. *Catheter Cardiovasc Interv* 2010;75:914-8.
 25. Macaya C, Serruys P, Ruygrok P, et al. Continued benefit of coronary stenting versus balloon angioplasty. One-year clinical follow-up of the BENESTENT Trial. *J Am Coll Cardiol* 1996;27:255-61.
 26. de Jaegere P, Mudra H, Figulla H, et al. Intravascular ultrasound-guided optimized stent deployment. Immediate and 6 months clinical and angiographic results from the Multicenter Ultrasound Stenting in Coronaries Study (MUSIC Study). *Eur Heart J* 1998;19:1214-23.
 27. Otake H, Shite J, Ako J, et al. Local determinants of thrombus formation following sirolimus-eluting stent implantation assessed by optical coherence tomography. *JACC Cardiovasc Interv* 2009;2:459-66.
 28. Suwannasom P, Sotomi Y, Ishibashi Y, et al. The Impact of Post-Procedural Asymmetry, Expansion, and Eccentricity of Bioresorbable Everolimus-Eluting Scaffold and Metallic Everolimus-Eluting Stent on Clinical Outcomes in the ABSORB II Trial. *JACC Cardiovasc Interv* 2016;9:1231-42.
 29. Mattesini A, Boeder N, Valente S, et al. Absorb vs. DESolve: an optical coherence tomography comparison of acute mechanical performances. *EuroIntervention* 2016;12:e566-73.
 30. Cook S, Eshtehardi P, Kalesan B, et al. Impact of incomplete stent apposition on long-term clinical outcome after drug-eluting stent implantation. *Eur Heart J* 2012;33:1334-43.
 31. Gogas BD, Bourantas CV, Garcia-Garcia HM, et al. The edge vascular response following implantation of the Absorb everolimus-eluting bioresorbable vascular scaffold and the XIENCE V metallic everolimus-eluting stent. First serial follow-up assessment at six months and two years: insights from the first-in-man ABSORB Cohort B and SPIRIT II trials. *EuroIntervention* 2013;9:709-20.
 32. Rodriguez-Granillo GA, Aoki J, Ong AT, et al. Methodological considerations and approach to cross-technique comparisons using in vivo coronary plaque characterization based on intravascular ultrasound radiofrequency data analysis: insights from the Integrated Biomarker and Imaging Study (IBIS). *Int J Cardiovasc Intervent* 2005;7:52-8.
 33. Bruining N, de Winter S, Roelandt JR, et al. Monitoring in vivo absorption of a drug-eluting bioresorbable stent with intravascular ultrasound derived parameters: a feasibility study. *JACC Cardiovasc Interv* 2010;3:449-56.
 34. Bruining N, Verheye S, Knaapen M, et al. Three-dimensional and quantitative analysis of atherosclerotic plaque composition by automated differential echogenicity. *Catheter Cardiovasc Interv* 2007;70:968-78.
 35. Brown AJ, Obaid DR, Costopoulos C, et al. Direct Comparison of Virtual-Histology Intravascular Ultrasound and Optical Coherence Tomography Imaging for Identification of Thin-Cap Fibroatheroma. *Circ*

- Cardiovasc Imaging 2015;8:e003487.
36. Maehara A, Cristea E, Mintz GS, et al. Definitions and methodology for the grayscale and radiofrequency intravascular ultrasound and coronary angiographic analyses. *JACC Cardiovasc Imaging* 2012;5:S1-9.
 37. Gogas BD, Serruys PW, Diletti R, et al. Vascular response of the segments adjacent to the proximal and distal edges of the ABSORB everolimus-eluting bioresorbable vascular scaffold: 6-month and 1-year follow-up assessment: a virtual histology intravascular ultrasound study from the first-in-man ABSORB cohort B trial. *JACC Cardiovasc Interv* 2012;5:656-65.
 38. Verheye S, Martinet W, Kockx MM et al. Selective clearance of macrophages in atherosclerotic plaques by autophagy. *J Am Coll Cardiol* 2007;49:706-15.
 39. Onuma Y, Serruys PW, Perkins LE, et al. Intracoronary optical coherence tomography and histology at 1 month and 2, 3, and 4 years after implantation of everolimus-eluting bioresorbable vascular scaffolds in a porcine coronary artery model: an attempt to decipher the human optical coherence tomography images in the ABSORB trial. *Circulation* 2010;122:2288-300.
 40. Karanasos A, Simsek C, Gnanadesigan M, et al. OCT assessment of the long-term vascular healing response 5 years after everolimus-eluting bioresorbable vascular scaffold. *J Am Coll Cardiol* 2014;64:2343-56.
 41. Serruys PW, Ormiston JA, Onuma Y, et al. A Bioabsorbable Everolimus-Eluting Coronary Stent System (ABSORB): 2-year outcomes and results from multiple imaging methods. *Lancet* 2009;373:897-910.
 42. Ormiston JA, Serruys PW, Regar E, et al. A bioabsorbable everolimus-eluting coronary stent system for patients with single de-novo coronary artery lesions (ABSORB): a prospective open-label trial. *Lancet* 2008;371:899-907.
 43. Asami M, Aoki K, Serruys PW et al. Feasibility of 320-row multi-detector computed tomography angiography to assess bioresorbable everolimus-eluting vascular scaffolds. *Cardiovasc Interv Ther* 2016;31:96-100.
 44. Onuma Y, Dudek D, Thuesen L. Five-year clinical and functional multislice computed tomography angiographic results after coronary implantation of the fully resorbable polymeric everolimus-eluting scaffold in patients with de novo coronary artery disease: the ABSORB cohort A trial. *JACC Cardiovasc Interv* 2013;6:999-1009.
 45. Suwannasom P, Onuma Y, Campos CM, et al. Fate of Bioresorbable Vascular Scaffold Metallic Radio-Opaque Markers at the Site of Implantation After Bioresorption. *JACC Cardiovasc Interv* 2015;8:1130-2.
 46. Ojeda S, Pan M, Suárez de Lezo J. Patency of coronary side branches covered by an everolimus-eluting bioresorbable vascular scaffold: clinical outcomes and computed tomography scan follow-up. *EuroIntervention* 2016;11:e1283-90.
 47. Zuin M, Rigatelli G, Scaranello F, et al. Follow-up of coronary artery patency after implantation of bioresorbable coronary scaffolds: The emerging role of magnetic coronary artery imaging. *Cardiovasc Revasc Med* 2017. [Epub ahead of print].
 48. Hickethier T, Kröger JR, Von Spiczak J, et al. Non-invasive imaging of bioresorbable coronary scaffolds using CT and MRI: First in vitro experience. *Int J Cardiol* 2016;206:101-6.
 49. Reiss S, Krafft AJ, Zehender M, et al. Magnetic resonance imaging of bioresorbable vascular scaffolds: potential approach for noninvasive evaluation of coronary patency. *Circ Cardiovasc Interv* 2015;8(4). pii: e002388.
 50. Barone-Rochette G, Vautrin E, Rodière M, et al. First magnetic resonance coronary artery imaging of bioresorbable vascular scaffold in-patient. *Eur Heart J Cardiovasc Imaging* 2015;16:229.

Cite this article as: Pernigotti A, Moscarella E, Spitaleri G, Scardino C, Ishida K, Brugaletta S. Methods to assess bioresorbable vascular scaffold devices behaviour after implantation. *J Thorac Dis* 2017;9(Suppl 9):S959-S968. doi: 10.21037/jtd.2017.06.110